

Sub-diffraction limited quantum imaging of a living cell

Michael A. Taylor,^{1,2} Jiri Janousek,³ Vincent Daria⁴, Joachim Knittel¹,
Boris Hage³, Hans-A. Bachor^{3,4}, and Warwick P. Bowen^{2*}

¹Department of Physics, University of Queensland, St Lucia, Queensland 4072, Australia

²Centre for Engineered Quantum Systems, University of Queensland, St Lucia,
Queensland 4072, Australia

³Department of Quantum Science, Australian National University, Canberra,
ACT 0200, Australia

⁴John Curtin School of Medical Research, Australian National University, Canberra,
ACT 0200, Australia

*To whom correspondence should be addressed; E-mail: wbowen@physics.uq.edu.au

Abstract

Quantum techniques allow the resolution constraints of classical imaging to be overcome, and are expected to have important applications in biology. We report the first demonstration of sub-diffraction limited quantum imaging in biology. Naturally occurring lipid granules of approximately 300 nm diameter are used to image the local mechanical properties of the cellular cytoplasm, with spatial resolution enabled by thermal diffusion. Spatial structure is resolved at length scales down to 10 nm. Our results confirm the longstanding prediction that use of quantum correlated light can enhance spatial resolution in biology, allowing a 14% enhancement over that achievable with coherent light. Combined with state-of-the-art sources of quantum correlated light, this technique provides a path towards an order of magnitude improvement in resolution over similar classical imaging techniques.

Quantum resources play an increasingly important role in precision measurements, and are applied in widely varying fields such as astrophysics [1], field sensing [2, 3, 4], and subcellular microscopy [5, 6, 7, 8]. They both allow classical constraints such as the shot-noise limit or diffraction limit to be overcome, and enable new engineered nanoprobe for sensing. Such advances are important in biological imaging, where any improvement in imaging technology can reveal new levels of cellular complexity. Since sub-cellular structures can have nanometer size scales, spatial resolution surpassing the diffraction limit is particularly beneficial. The realization of sub-diffraction limited quantum imaging in biology is therefore a longstanding and important challenge.

Here we demonstrate sub-diffraction limited biological imaging with quantum enhanced resolution. To achieve this result, a new approach to quantum imaging is developed which applies squeezed states of light within a classical sub-diffraction limited imaging technique. Together this allows cellular structure to be imaged at length scales down to 10 nm. For fixed optical power, squeezed light provides 14% enhancement over the resolution possible with classical imaging, demonstrating for the first time that non-classical light can improve resolution in biology. Alternatively, a 42% reduction in optical power is possible without compromising resolution, with consequent reduction in damage [9, 10] and photochemical disruption of cellular processes [10, 11].

This first quantum image of the structure within a living cell complements other recent applications of quantum imaging in biology, with Nitrogen Vacancy (NV) nanodiamonds allowing thermal [7] and magnetic imaging [6, 12, 13], and quantum correlated light allowing dispersion compensation [14]. Prior to the results presented here, all biological applications of quantum imaging have been diffraction limited, including NV based cellular imaging

which has relied on optically resolvable arrays of stationary NV probes [6, 7, 12, 13], confining it to the study of relatively large cellular structures and organelles. The resolution achieved here is over an order of magnitude finer than in previous biological quantum imaging experiments, providing the possibility to observe important nanoscale cellular structures such as membranes, actin networks, and individual proteins. Since the approach is in principle transferrable to NV based imaging, it could also open the door to simultaneous sub-diffraction limited imaging of viscoelasticity, temperature and magnetic fields.

In the imaging technique introduced here, the local structure of the cell is interrogated non-invasively via its effect on the thermal motion of naturally occurring nanoparticles as they diffuse around the cell. In a purely viscous medium such as water, these particles would follow well-known diffusive Brownian motion. By contrast, the cytoplasm in a cell is structured and crowded with proteins and other macromolecules which confine particle motion and slow the thermal motion [15]. The resulting subdiffusive motion characterizes the viscoelasticity of the cytoplasm [16, 17, 19, 18]. Thermal motion is crucial to the operation of the cell, mediating many important processes. For instance, subdiffusion slows the initial approach of chemical reactants to one another but also decreases the likelihood that they will pass without interacting, which improves the efficiency of the reaction [19, 20, 21]. Subdiffusion also has a strong effect on enzyme reactions [22, 23], and the formation of spatiotemporal patterns [24, 25]. The technology introduced here allows improved observation of spatial variations in subdiffusive motion, and is thereby an enabling step towards a better understanding of the nanoscale structure within a cell. Although the biological implications of such structure are not yet fully understood, it has been shown that the optimal diffusive regime is different for storage, transport, and chemical reactions [20]. As such, nanoscale structural variations could potentially reflect the function of small regions of the cytoplasm.

The experiment builds upon the recently developed quantum enhanced nanoparticle tracking technique described in Ref. [8]. In that work, temporal fluctuations in cellular viscoelasticity were monitored with quantum enhanced precision via optical centroid measurements [26, 27]. However, the possibility to use diffusion to achieve spatial resolution, and thereby image the cell, was not examined. As a result fluctuations caused by time-dynamic processes within the cell could not be distinguished from those due to nanoscale structure that the particle is exposed to as it diffuses around the cell. Nor was it possible to retrieve any quantitative information about the spatial structure. These limitations are resolved here by tracking nanoparticles with sub-nm precision as they explore an extended region of the cell, and analyzing spatial variations in the subdiffusive motion. The experimental setup (shown in Fig. 1A) features several important modifications from a conventional optical particle tracking experiment, facilitating the use of amplitude squeezed light to enhance measurement sensitivity. Because most biological processes occur at Hz-kHz frequencies, where classical noise sources constrain the possibility of generating squeezing [28], a novel optical lock-in technique [29] is used to evade low frequency noise and allow quantum enhancement at these frequencies. This is combined with dark-field illumination [30, 31] to remove unwanted light from the measured optical field. Additionally, self-homodyne measurement is used, which allows the local oscillator itself to be squeezed, such that the squeezed field perfectly overlaps with the local oscillator at detection even without prior knowledge of the spatial mode shape after propagation through the living cell and high numerical aperture lenses.

Saccharomyces cerevisiae yeast cells were immobilized with an optical trap, and the motion of lipid granules within the cellular cytoplasm was tracked with either squeezed or coherent light [8]. The high frequency thermal motion of a lipid granule then reveals the viscoelastic properties of the surrounding cytoplasm, while for sufficiently long measurements its slow thermal drift provides spatial resolution by bringing it into contact with different parts of the cellular cytoplasm. Thus, spatial inhomogeneity in the viscoelasticity can be quantified by a single continuous measurement of the lipid granule position. In our experiment, the particle position $x(t)$ was measured by combining scattered light from the sample with a local oscillator field which was spatially shaped such that direct measurement of the total power yielded the particle position (Fig. 1B). In the same manner as in Ref. [8], the local viscoelasticity of the cytoplasm could be determined from the mean squared displacement (MSD) of the particle after a delay τ ,

$$\langle \Delta x^2(\tau) \rangle = \langle (x(t) - x(t - \tau))^2 \rangle, \quad (1)$$

with an example shown in Fig. 1C. The corresponding spectra (Fig. 1C inset) shows that squeezed light lowers the

noise floor of the measurement by 2.4 dB. For short delays, the MSD is dominated by thermal motion and has the form

$$\langle \Delta x^2(\tau) \rangle = 2D\tau^\alpha, \quad (2)$$

where the diffusive parameter α carries information about mechanical properties of the surrounding medium [32, 33]. α is determined for a set of data by fitting the MSD at short delays to Eq. 2. When $\alpha = 1$, the motion is diffusive, which is indicative of a random walk type of motion, whereas confinement of the particle causes subdiffusive motion ($0 < \alpha < 1$). In our experiments, 100 ms of data was sufficient to precisely determine α . Subdiffusive motion is an indicator that the cellular cytoplasm exhibits both viscosity and elasticity [16, 17, 19, 18], since to constrict motion the cytoplasm must store mechanical energy. Consequently, the measured values of α allowed temporal variations in the cellular viscoelasticity to be characterized with 10 Hz bandwidth.

As lipid particles undergo three dimensional (3D) thermal motion, they are exposed to different parts of the cell (Fig. 1B inset). Since our experiments provide both α and the mean position of the particle along the x axis, it is possible to construct 1D images of α which follow the projection of the 3D trajectory onto the x axis (see Fig. 2), and map out the physical structure within the cellular cytoplasm. To construct such images, a series of experiments were performed in which the nanoparticle motion was tracked as it diffused through an extended region of the cell. The data from each experiment was separated into 100 ms segments, with both α and the mean position along the x axis determined for each segment. As the particle diffused, an image of α could thereby be created as a function of x , as shown in Fig. 2. The directly obtained images exhibited substantial noise both from the measurement process and due to the unknown trajectory of the particle in the y and z directions. To identify statistically resolvable features, the running mean and standard error of α were calculated along the x axis, with spatial resolution given by the size of the averaging window. As shown in the supplementary information, an analysis of the correlations between subsequent images allowed confirmation that the variations in α arise predominantly from spatial structure rather than dynamical processes within the cell (Supplementary section S1), and also allowed the local characteristic length scale of the viscoelastic structure to be determined with 2 nm precision.

Since increased spatial averaging makes small changes in α easier to resolve, an intrinsic compromise is present between image contrast and spatial resolution. In this Letter, the choice of 10 nm spatial resolution was found to provide sufficient contrast to observe cellular structure. Four example images are shown in Fig. 2, with clear spatial structure evident even at the 10 nm spatial resolution limit. The observed spatial dependence shows a number of different behaviors because, for each image of $\alpha(x)$, the particle follows a different 3D trajectory. These include gradual linear changes in α (e.g. Fig. 2A) which suggest a spatial gradient in the molecular crowding along the x axis, narrow dips in α (e.g. Fig. 2B at 40 nm) suggestive of barriers in the cytoplasm, areas of homogeneity (e.g. Fig. 2C), and peaks in α (e.g. Fig. 2D at -55 nm) which may follow from small voids in the cytoplasmic structure.

To characterize the spatial resolution of the imaging procedure and to exclude the possibility that the observed spatial variations in α were due to experimental drifts, similar images were constructed for 1 μm radius silica beads in water. The resulting images (Fig. 3) show no statistically significant spatial structure, with $\alpha = 1$ at all spatial locations as expected for Brownian motion. Since water is homogeneous with $\alpha = 1$ throughout, the variation in this data allows the statistical uncertainty of our measurements of α to be determined. The spatial resolution was characterized by varying the width of the running average along x as shown representatively in Fig. 3A to C. As the width increases, the spatial resolution is degraded, but the inclusion of more data allows improved precision in determining α . The overall precision in α is plotted as a function of resolution in Fig. 3D for data recorded with both squeezed and coherent light, which shows that for fixed sensitivity, the reduced measurement noise achieved with squeezing enables 14% enhanced spatial resolution (Fig. 3E). For instance, from a 10 s data set, biological structures that change α by 0.1 are unresolvable using coherent light if their size is smaller than 12 nm. Using squeezed light they may be resolved at sizes down to 10 nm.

Since only the projection of the particle motion onto the x axis is tracked in our current experiments, it is not possible to define the complete trajectory along which the 1D images are taken. By incorporating our technique in a standard 3D particle tracking setup [34] it would be possible to map the complete 3D trajectory. A quantum enhanced 3D image of the cell could then be generated at nanoscale, with quantum enhancement only required

for one axis from which α could be determined. Furthermore, an extended field of view could be achieved by increasing the measurement length and thus allowing the particle more time to diffuse, or by applying an optical trapping force to the particle to move it into new regions of the cell.

As is typical of nanoprobe based microscopy techniques, the spatial resolution of the images produced here is not fundamentally constrained by the diffraction limit. Since the intracellular medium interacts with the nanoparticle across its entire surface area, it might be thought that the particle diameter sets a fundamental resolution limit. However this is not the case, as can be appreciated from an analogy to atomic force microscopy (AFM). In AFM, the transverse resolution is constrained by the tip size. However, the vertical resolution can be far superior[35], and is fundamentally constrained only by short range forces[35] and measurement signal-to-noise. Similarly, the resolution of the imaging technique introduced here is limited to the particle diameter in directions transverse to its trajectory; while in the direction of particle motion far superior resolution is possible, fundamentally limited only by measurement noise [27, 36] and the range of viscoelastic forces from structure in the cell. Consequently, along the trajectory of the particle, the location of structure within the cell may be established with precision far smaller than the particle diameter. Over time, diffusion acts to drive the particle through the cellular structure on a range of trajectories, which combined with 3D tracking, in principle enables nanometer resolution along all three axes.

The resolution enhancement reported here could be substantially improved using an increased level of squeezing. Squeezing in excess of 10 dB has been directly measured in a number of experiments [37, 38]. Using this level of measured squeezing, more an order of magnitude enhancement should be feasible, allowing Angström level precision (Supplementary section S2). In principle, further enhancement may be possible by using an array of photon number resolving detectors, with recent theoretical results predicting that this approach could even allow particle tracking at the de Broglie limit [26]. Such a resolution enhancement would be greatly beneficial in biological imaging. By comparison, widely used classical super-resolution techniques such as stimulated emission depletion (STED) microscopy are currently limited to spatial resolution of a few tens of nanometers within cells [39, 40].

We report the first demonstration of sub-diffraction limited biological quantum imaging, and demonstrate that non-classical light can improve spatial resolution in biological applications. The viscoelastic structure within a living yeast cell is imaged along the trajectory of a thermally driven nanoparticle, revealing spatial structure with length scales down to 10 nm. The use of squeezed light was found to enhance the spatial resolution by 14%. Future experiments which apply this method with improved squeezing technology are expected to resolve sub-nm structure.

References

- [1] J. Abadie *et al.*, A gravitational wave observatory operating beyond the quantum shot-noise limit. *Nature Phys.* **7**, 962–965 (2011).
- [2] J. R. Maze *et al.*, Nanoscale magnetic sensing with an individual electronic spin in diamond. *Nature* **455**, 644–647 (2008).
- [3] G. Balasubramanian *et al.*, Nanoscale imaging magnetometry with diamond spins under ambient conditions. *Nature* **455**, 648–651 (2008).
- [4] F. Dolde *et al.*, Electric-field sensing using single diamond spins. *Nature Phys.* **7**, 459–463 (2011).
- [5] L. P. McGuinness *et al.*, Quantum measurement and orientation tracking of fluorescent nanodiamonds inside living cells. *Nature Nanotech.* **6**, 358–363 (2011).
- [6] D. Le Sage *et al.*, Optical magnetic imaging of living cells. *Nature* doi:10.1038 (2013).
- [7] G. Kucsko *et al.*, Nanometer scale quantum thermometry in a living cell. arXiv:1304.1068 (2013).
- [8] M. A. Taylor *et al.*, Biological measurement beyond the quantum limit. *Nature Photon.* **7**, 229–233 (2013).

- [9] E. J. Peterman, F. Gittes, C. F. Schmidt, Laser-induced heating in optical traps. *Biophys. J.* **84**, 1308–1316 (2003).
- [10] K. C. Neuman, E. H. Chadd, G. F. Liou, K. Bergman, S. M. Block, Characterization of photodamage to *Escherichia coli* in optical traps. *Biophys. J.* **77**, 2856–2863 (1999).
- [11] R. Lubart, R. Lavi, H. Friedmann, S. Rochkind, Photochemistry and photobiology of light absorption by living cells. *Photomed. Laser Surg.* **24**, 179–185 (2006).
- [12] S. Steinert *et al.*, Magnetic spin imaging under ambient conditions with sub-cellular resolution. *Nat. Commun.* **4**, 1607 (2013).
- [13] S. Kaufmann *et al.*, Detection of atomic spin labels in a lipid bi-layer using a single-spin nanodiamond probe. arXiv:1304.3789 (2013).
- [14] M. B. Nasr *et al.*, Quantum optical coherence tomography of a biological sample. *Opt. Commun.* **282**, 1154–1159 (2009).
- [15] M. Weiss, M. Elsner, F. Kartberg, T. Nilsson T, Anomalous subdiffusion is a measure for cytoplasmic crowding in living cells. *Biophys. J.* **87**, 3518–3524 (2004).
- [16] I. M. Tolić-Nørrelykke, E. L. Munteanu, G. Thon, L. Oddershede, K. Berg-Sørensen, Anomalous diffusion in living yeast cells. *Phys. Rev. Lett.* **93**, 078102 (2004).
- [17] C. Selhuber-Unkel, P. Yde, K. Berg-Sørensen, L. B. Oddershede, Variety in intracellular diffusion during the cell cycle. *Phys. Biol.* **6**, 025015 (2009).
- [18] G. Guigas, C. Kalla, M. Weiss, Probing the nanoscale viscoelasticity of intracellular fluids in living cells. *Biophys. J.* **93**, 316–323 (2007).
- [19] E. N. Senning, A. H. Marcus, Actin polymerization driven mitochondrial transport in mating *S. cerevisiae*. *Proc. Natl. Acad. Sci. USA* **107**, 721–725 (2010).
- [20] G. Guigas, M. Weiss, Sampling the cell with anomalous diffusion—the discovery of slowness. *Biophys. J.* **94**, 90–94 (2008).
- [21] S. Condamin, V. Tejedor, R. Voituriez, O. Bénichou, J. Klafter, Probing microscopic origins of confined subdiffusion by first-passage observables. *Proc. Natl. Acad. Sci. USA* **105**, 5675–5680 (2008).
- [22] H. Berry, Monte carlo simulations of enzyme reactions in two dimensions: fractal kinetics and spatial segregation. *Biophys. J.* **83**, 1891–1901 (2002).
- [23] S. Schnell, T. E. Turner, Reaction kinetics in intracellular environments with macromolecular crowding: simulations and rate laws. *Prog. Biophys. Mol. Biol.* **85**, 235–260 (2004).
- [24] M. Weiss, Stabilizing Turing patterns with subdiffusion in systems with low particle numbers. *Phys. Rev. E.* **68**, 036213 (2003).
- [25] M. Weiss, T. Nilsson, In a mirror dimly: tracing the movements of molecules in living cells. *Trends Cell Biol.* **14**, 267–273 (2004).
- [26] M. Tsang, Quantum imaging beyond the diffraction limit by optical centroid measurements. *Phys. Rev. Lett.* **102**, 253601 (2009).
- [27] M. I. Kolobov, C. Fabre, Quantum limits on optical resolution. *Phys. Rev. Lett.* **85**, 3789–3792 (2000).

- [28] K. McKenzie *et al.*, Squeezing in the audio gravitational-wave detection band. *Phys. Rev. Lett.* **93**, 161105 (2004).
- [29] M. A. Taylor, J. Knittel, W. P. Bowen, Optical lock-in particle tracking in optical tweezers. *Opt. Express* **21**, 8018-8024 (2013).
- [30] S. Kudo, Y. Magariyama, S. I. Aizawa, Abrupt changes in flagellar rotation observed by laser dark-field microscopy. *Nature* **346**, 677–680 (1990).
- [31] M. Nishiyama, E. Muto, Y. Inoue, T. Yanagida, H. Higuchi, Substeps within the 8-nm step of the ATPase cycle of single kinesin molecules. *Nat. Cell Biol.* **3**, 425–428 (2001).
- [32] F. Gittes, B. Schnurr, P. D. Olmsted, F. C. MacKintosh, C. F. Schmidt, Microscopic viscoelasticity: shear moduli of soft materials determined from thermal fluctuations. *Phys. Rev. Lett.* **79**, 3286–3289 (1997).
- [33] T. G. Mason, K. Ganesan, J. H. Van Zanten, D. Wirtz, S. C. Kuo, Particle tracking microrheology of complex fluids. *Phys. Rev. Lett.* **79**, 3282–3285 (1997).
- [34] A. Pralle, M. Prummer, E.-L. Florin, E. H. K. Stelzer, J. K. H. Hörber, Three-dimensional high-resolution particle tracking for optical tweezers by forward scattered light. *Microsc. Res. Tech.* **44**, 378–386 (1999).
- [35] D. J. Müller, A. Engel, The height of biomolecules measured with the atomic force microscope depends on electrostatic interactions. *Biophys. J.* **73**, 1633-1644 (1997).
- [36] M. A. Taylor, J. Knittel, W. P. Bowen, Fundamental constraints on particle tracking with optical tweezers. *New J. Phys.* **15**, 023018 (2013).
- [37] M. S. Stefszky *et al.*, Balanced homodyne detection of optical quantum states at audio-band frequencies and below. *Class. Quantum Grav.* **29**, 145015 (2012).
- [38] M. Mehmet *et al.*, Observation of squeezed states with strong photon-number oscillations. *Phys. Rev. A* **81**, 013814 (2010).
- [39] K. I. Willig *et al.*, Nanoscale resolution in GFP-based microscopy. *Nat. Methods* **3**, 721–723 (2006).
- [40] R. Schmidt *et al.*, Spherical nanosized focal spot unravels the interior of cells. *Nat. Methods* **5**, 539–544 (2008).
- [41] Y. Tseng, J. S. Lee, T. P. Kole, I. Jiang, D. Wirtz, Micro-organization and visco-elasticity of the interphase nucleus revealed by particle nanotracking. *J. Cell Sci.* **117**, 2159–2167 (2004).

Acknowledgments: This work was supported by the Australian Research Council Discovery Project Contract No. DP0985078 and the Australian Research Council Centre of Excellence for Engineered Quantum Systems CE110001013.

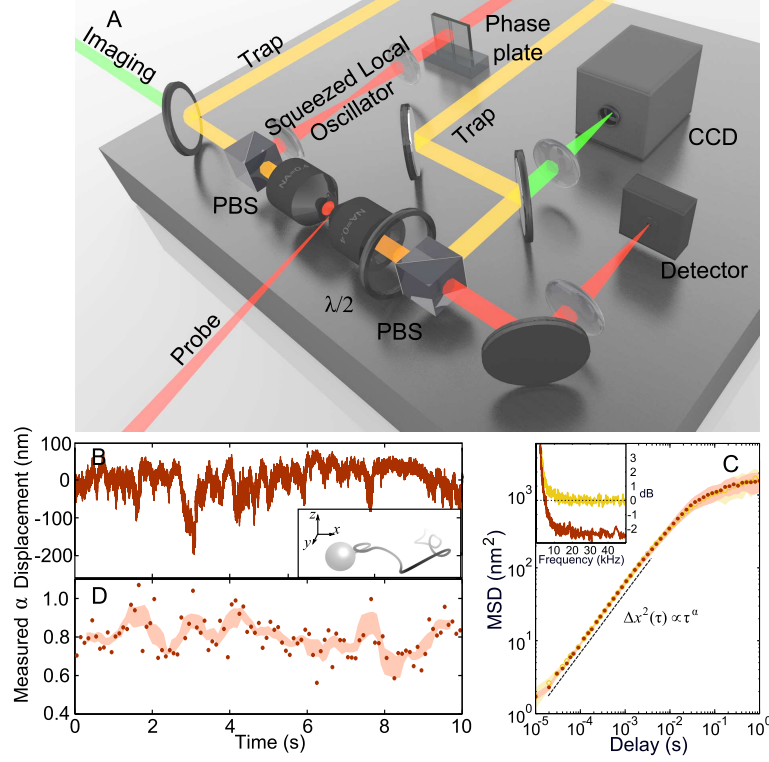


Figure 1: Experimental setup. (A) Counter-propagating trapping fields (orange) confine particles between two objectives, and are isolated from the detector with polarizing beamsplitters (PBS) and waveplates ($\lambda/2$). An imaging field (green) allows visual identification of the particles near the optical trap on a CCD camera. The particle tracking measurement relies only on an amplitude squeezed local oscillator and an amplitude modulated probe (red), with the probe providing dark-field illumination, and the particle tracking signal arising from interference between scattered light from the probe and the local oscillator. (B) Measured particle motion, which is the x projection of the 3D motion (shown schematically in the inset). (C) The MSD is constructed with both squeezed light (dark red) and coherent light (gold), and α determined by fitting this to Eq. 2. The classical and squeezed example traces here both yield $\alpha = 0.83$. The normalized spectral density is plotted in the inset, which shows that squeezing suppressed the noise floor by 2.4 dB. (D) The raw data was divided into 100 ms segments and the value of α established for each (solid dots). The light red shaded region represents the moving mean and standard error with a 0.5 second width.

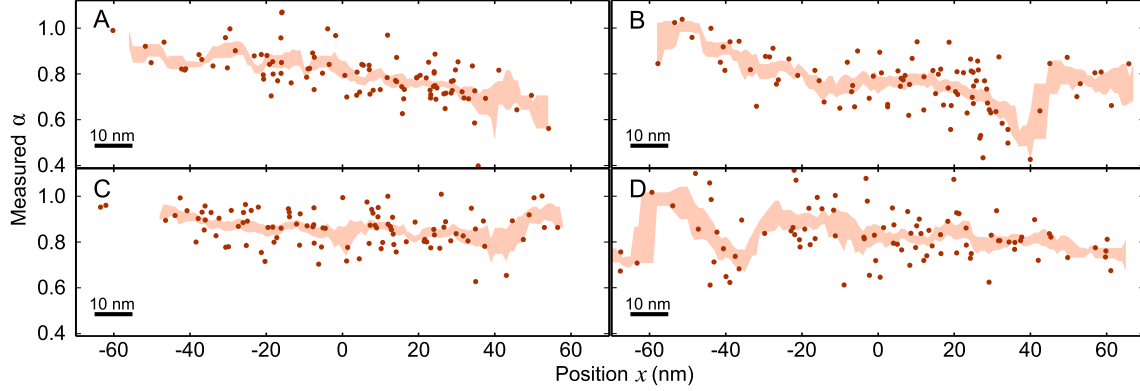


Figure 2: Images of α . Each circle represents a single measurement of α vs x using a 100 ms set of data. The shaded regions represent the running mean and standard error with 10 nm resolution (thick black bar). The images (A–D) were recorded minutes apart, which allowed the particle time to diffuse to different regions of the cell, with qualitatively different spatial structures. The particle confinement is greatest where α is lowest, such as the dip about 40 nm in (B), and the particle movement is most free when α is highest, such as the peak at -55 nm in (D).

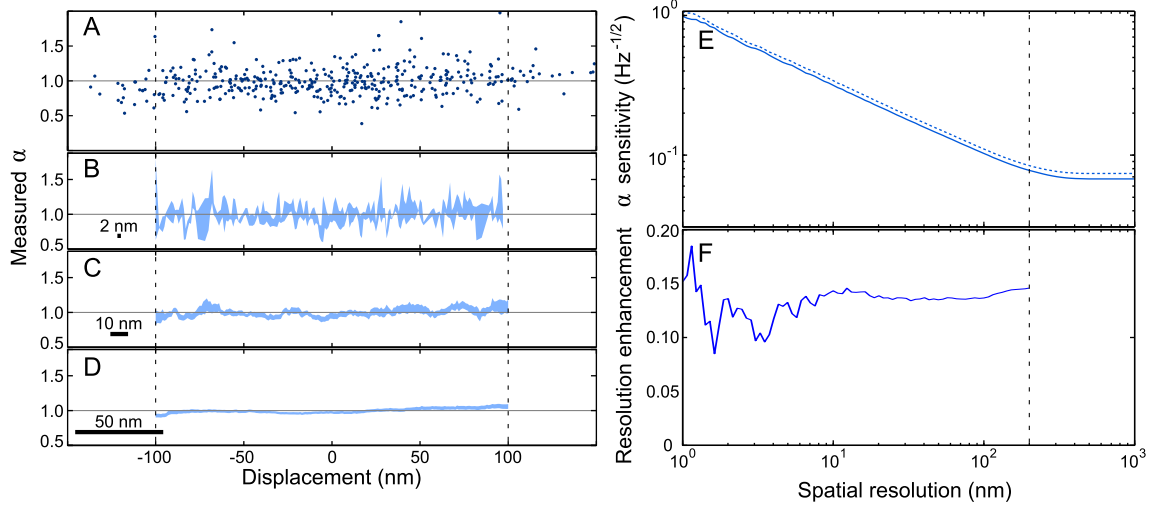


Figure 3: To calibrate the quantum enhancement achieved here, an image of α was constructed from particles in water. The measurements of α vs. x are shown in (A). (B–D) show the corresponding moving mean and standard error calculated over a 200 nm range with spatial resolution of 2 nm, 10 nm, and 50 nm, respectively. The data closely follows the expected $\alpha = 1$ result (horizontal line). The number of independent spatially resolved points decreases as the spatial resolution is broadened, while the increased spatial averaging allows a more precise determination of α . (E) The precision with which α could be determined is plotted as a function of spatial resolution for data recorded with both squeezed (solid line) and coherent (dashed line) light. Since the number of points being averaged is proportional to the spatial resolution, the precision scales as the inverse square root of spatial resolution until the averaging window width becomes comparable to the spatial range of the measured data. When resolving features of a fixed amplitude in α , squeezing allows enhanced spatial resolution as shown in (F), with approximately 14% narrower spatial resolution available over most of the measurable range. Outside the vertical dashed lines in (A–F), there was insufficient data to construct an image.

Supplementary Materials

S1: Correlation analysis of images

It is important to rigorously establish whether the changes in α measured here result from particle motion within nanoscale structure or from time-dependent cellular processes. Because the trajectory over which α is imaged differs in each run of the experiments reported here, different images correspond to different regions of the cell. However, when spatial images are produced within a short time of one another, the corresponding trajectories are not spatially separated by a substantial distance, and the images should retain some correlations. By contrast, any temporal contributions to the measured $\alpha(x)$ should be completely uncorrelated between subsequent images. Thus, analysis of the correlations between subsequent images can determine whether temporal fluctuations or spatial structure in α are dominant. The correlations which result from spatial structure can be predicted with a simple model which assumes that α is perfectly correlated if the displacement dr along the y and z axes is below the length scale of structural variations r_c , and completely uncorrelated if $dr > r_c$. Then, assuming that the motion along each axis independently follows Eq. 2, and also assuming Gaussian probability distributions, the average correlation is given by the probability that the particle remains within r_c

$$P(dr < r_c) = 1 - \text{Exp} \left[-\frac{\pi r_c^2}{4 \langle dr^2 \rangle} \right] = 1 - \text{Exp} \left[-\frac{\pi}{4} \left(\frac{dt}{T_c} \right)^{-\alpha} \right], \quad (3)$$

where T_c is the average time that the particle takes to diffuse into an uncorrelated region of the cell, such that $\langle dr^2 \rangle = r_c^2$. To determine whether the experimental data follows Eq. 3, a series of $\alpha(x)$ images were constructed, and the correlations between the subsequent images calculated as a function of delay (Fig. S1). This experimental data was fitted to Eq. 3 with T_c and α used as fitting parameters. The data shows excellent agreement with the simple model, which confirms that the measured changes in α are spatial rather than temporal. This is consistent with observations from other types of cell that have found the viscoelasticity to vary spatially by an order of magnitude [41], which is much larger than the temporal variations produced through cellular processes [17]. Furthermore, by quantifying the time constant T_c , the characteristic local length scale of viscoelastic structure can be determined in the region of the nanoparticle. To test whether this length scale varies across the cell, the correlation analysis described above was carried out with three separate sets of data, as shown in Fig. S1. Assuming the diffusion follows the MSD measured in Fig. 2C, the length scales of the viscoelastic structure in each region were determined to be 46.9 ± 1.3 nm, 43.7 ± 2.4 nm, and 42.6 ± 1.9 nm. This demonstrates that changes in the characteristic length of spatial structure in different parts of the cell can be statistically distinguished.

S2: Theoretically predicted quantum enhancement

Here the enhancement in spatial resolution achievable with squeezed light is determined by analyzing simulated data. The data analysis in the main text is performed as follows. A discrete series of measurements x_n of the particle position x are performed at evenly spaced intervals dt in time, where n is the measurement number. These are used to determine the mean squared displacement (MSD), by the relationship

$$\langle \Delta x^2(\tau = m dt) \rangle_{\text{exp}} = \sum (x_{n+m} - x_n)^2 - N_{\text{MSD}}, \quad (4)$$

where N_{MSD} is the mean variance. Although the expectation value of this experimental MSD is given by $2D\tau^\alpha$ (Eq. 2 of the main text), a single trajectory will only asymptote towards this in the limit of infinite statistically independent measurements. The number of statistically independent measurements at any delay τ is given by T/τ , where T is the total measurement time. As such, even a perfectly noise-free determination of the particle motion cannot yield α with complete certainty in a finite measurement time. Thus, the stochastic nature of the MSD introduces an intrinsic uncertainty into the value of α in addition to any uncertainty associated with the measurement noise. This intrinsic uncertainty is greatest at long delays, where the number of independent measurements is

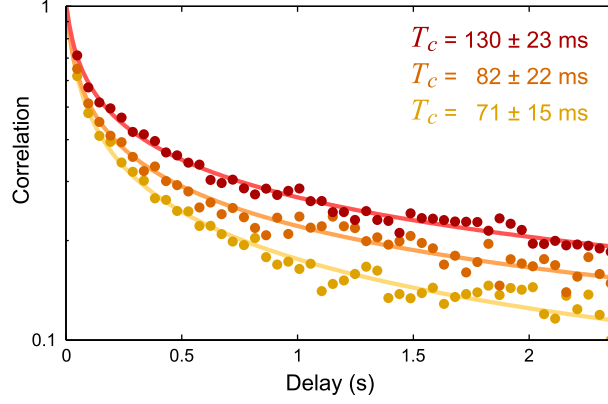


Figure S1: Correlation between a series of measured sets of $\alpha(x)$ as a function of the time separation between the data sets. The correlation decays in time because of the unknown motion along the y and z axes. The circles are experimentally determined correlations between a series of measurements, and the lines fit the data to Eq. 3, which determines the probability that subsequent measurements sample the same spatial environment. α was optimized to minimize the mean square error for a range of T_c . From this the optimal T_c was found, with the uncertainty corresponding to the change in T_c which doubles the mean square error.

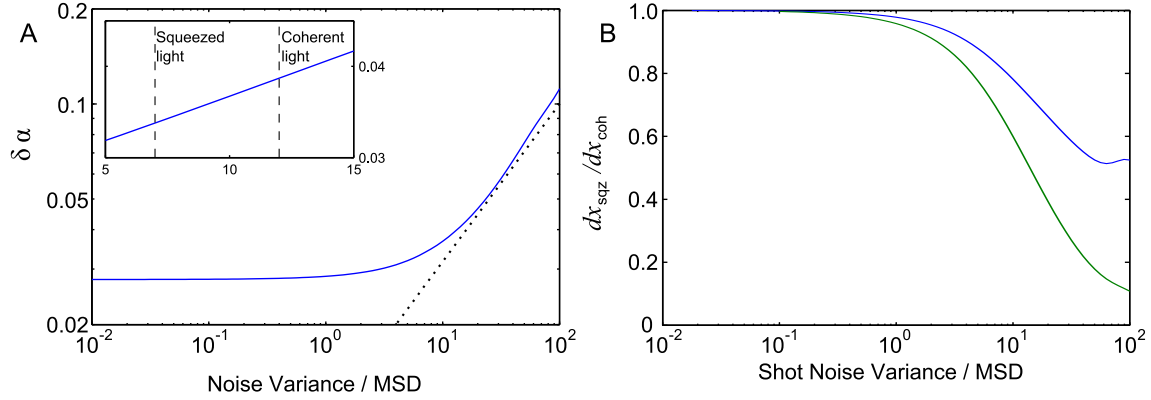


Figure S2: The influence of measurement noise in viscoelastic imaging. (A) The precision with which α can be determined ($\delta\alpha$) is plotted against the measurement noise variance, normalized to the MSD at minimum delay. The dotted line scales as the square root of the noise variance, and approximately follows $\delta\alpha$ between variances of 10 and 100. The inset zooms in on this result in the regime of the experiments here, with the vertical dashed lines showing the noise variance on the experimental data. (B) The ratio of the spatial resolutions achievable with squeezed light and coherent light, with either 2.4 dB (blue) or 10 dB (green) of squeezing.

lowest. Measurement noise, by contrast, is of approximately constant amplitude with delay, and therefore has the greatest relative effect at short delays where the expectation value of the MSD is smallest.

The precision of any determination of α depends on both the intrinsic stochastic uncertainty and the measurement noise, such that the enhancement in α precision which may be achieved via squeezed light cannot be simply related to the noise suppression. To quantitatively predict the enhancement achievable, we perform Monte Carlo simulations, in which 10000 particle trajectories are simulated by a normally distributed random walk. Varying levels of white measurement noise are added to the trajectories, after which the MSD is calculated and α determined. The uncertainty $\delta\alpha$ is then given by the deviations of the predicted α from the ideal result of $\alpha = 1$ which should follow from such a random walk.

By repeating this for various levels of measurement noise, we could plot the uncertainty in α as a function of the measurement noise variance (Fig. S2A). In this case, the measurement length and fitting range matched the measurement conditions of the main text, and the noise variance was normalized to the MSD at minimum delay. When the noise is far smaller than the MSD (below 1 in Fig. S2A), the stochastic walk dominates the uncertainty in α , and techniques for noise reduction such as squeezing yield little improvement. When the measurement noise dominates the MSD at all analyzed delays, α cannot be determined with any reliability. As such, this region is not included in Fig. S2. Between these two extremes, measurement noise only dominates the MSD at short delays, and the precision with which α can be determined scales approximately as the square root of the noise variance. The relative contribution of shot noise increases as the measurement rate increases or the measurement duration decreases, both of which are required to produce high precision images, or if the optical power is reduced. As such, quantum enhanced precision provides maximal enhancement in the regime which is both most challenging to reach in classical experiments and most relevant to biological imaging.

When performing spatially resolved experiments, the precision with which α can be determined at a specific location is given by $\delta\alpha_{\text{image}} = \delta\alpha N^{-1/2}$, where N is the mean number of data points averaged at each location. For 1D imaging, this is given by

$$N = N_{\text{tot}} \frac{dx}{x_{\text{FOV}}}, \quad (5)$$

where N_{tot} is the total number of measurements of α , x_{FOV} is the field of view, and dx is the spatial resolution. Thus, if a fixed precision $\delta\alpha_{\text{image}}$ is required in a 1D image, the spatial resolution scales as $dx \propto \delta\alpha^2$. Using this, the spatial resolution enhancement is plotted in Fig. S2B for both 2.4 dB and 10 dB of measured squeezing.

At the noise levels measured here, we can predict that 2.4 dB of measured squeezing should have allowed 21% narrower spatial resolution in our experiment, which is greater than the measured 14% enhancement. The discrepancy between predicted and achieved enhancements may be due to the technical noise in the experiment such as low frequency noise and unwanted inclusion of RF modulations that were used for phase locking of the squeezing cavity. If the measurement rate were increased, such that the shot noise variance was 100 times greater than the MSD at minimum delay, 2.4 dB of measured squeezing would allow a 45% reduction in spatial resolution. If state-of-the art squeezing were used and the measured squeezing reached 10 dB, the quantum enhancement could then provide 90% narrower spatial resolution. Alternatively, an even greater measurement rate could sufficiently increase the measurement noise to preclude determination of α from a classical experiment, while α could still be determined with squeezed light.